Defence Science Journal, Vol. 58, No. 2, March 2008, pp. 227-237

Perforation of Layered Composite Plates by Impactors of Different Nose Shapes

R. Velmurugan[1] and N.K. Gupta[2]

[1]*Indian Institute of Technology Madras, Chennai–600 036*
[2]*Indian Institute of Technology Delhi, New Delhi–110 016*

ABSTRACT

Conical and hemispherical nose-shaped cylindrical impactors have been used in drop weight impact experiments on 3.1 mm CSM-polyester laminated plates. Based on experimental results, various failure mechanisms and energy absorbed in different failure modes are identified and calculated. It is found that the damage area beyond a certain value of impact energy does not increase. The perforation geometry is the same as that of the impactor irrespective of increased crack length, and complete rotation of petals takes place at impactors radius. It is also observed that the crack length increases with decrease in contact area. But, when the nose is sharp (5 mm hemispherical nose), there is no extended crack beyond perforated region. Blunt nosed (truncated conical impactor with 10 mm nose dia) impactors cause more number of petals/cracks than 10 mm hemispherical nosed impactor and less than 5 mm hemispherical nosed impactor. The petals formed by a cylindrical impactor with 40 mm hemispherical nose are unequal in size, whereas in the case of conical impactors, these are equal. At lower energies, blunt nosed impactors cause more delamination than the hemispherical ones, and at higher energy, it is the reverse. It is found that there exist many visible concentric circular ring hinge mechanisms at the top surface of plates.

Keywords: Composite plates, impact, penetration, nose shapes, energy absorption

NOMENCLATURE

U_{hoop}	Hoop strain energy
σ_y	Breaking tensile stress
a	Maximum crack length
ε_h	Maximum tensile strain
ε_d	Maximum shear strain
h_o	Thickness of plate
B	Width of petal at root
n	Number of petals
M_p	Plastic bending moment
$\theta_2 - \theta_1$	Petal rotation during plastic work
U_{del}	Total delamination energy
τ	Maximum shear stress
δ_d	Maximum shear displacement
l	Penetrated length of impactor
T	Hoop tension
Z_p	Plastic section modulus
U_f	Frictional energy
P	Impactor pullout force

Received 31 October 2007

1. INTRODUCTION

Composite structures in the form of layers are extremely susceptible to crack initiation and propagation in various failure modes. Analytical models capable of predicting the amount of energy absorbed in a laminated composite plate and its failure mechanism during impactor penetration, are of substantial practical value. While higher energy impact loading causes complete perforation or damage which is detectable on the surface, low energy impact produces extensive subsurface delamination. Much work has been carried out in the past to understand the phenomenon[1-4]. Attention has been directed towards understanding the cause and failure mechanisms of possible modes of failure due to impact loading, such as, matrix deformation and microcracking, interfacial debonding, lamina splitting, delamination, fibre breakage, and fibre pullout.

Delamination is one of the most prevalent crack growth modes in laminated composites as it causes severe reduction in strength and stiffness. Experimental investigations by Choi and Chang[2] and by Davis[3] showed that there exists a threshold impact energy below which there is no delamination in the laminate. When the energy is just above this level, delamination takes place instantaneously due to the interlaminar shear stress developed due to bending of the plate, and the delamination area increases continuously with the increase in impact energy. However, the subsequent increase in delamination size with the increase in impact energy is relatively slow. A combination of static and dynamic aspects of the energy terms are used by Landkof[4] to study the energy absorbed in the petal formation during penetration of thin plates by cylindro-conical impactors.

To compute the total energy absorbed by a laminated composite plate during petalling, all modes of failure of the structure should be considered. It has been assumed in the previous investigations that the energy absorbed by friction and plate bending can be neglected when compared to the plastic work[4]. Only limited information is available on the frictional behaviour of composite plate and impactor even though it is critical in the perforation process of composites. Present study reveals that frictional energy in laminated composites is significant and can not be neglected.

Gupta and Madhu[5] have studied the perforation and petal formation of plates during normal and oblique impact and found that the failure behaviour changes with the angle of impact. The studies by Corran[6], *et al.* and Johnson[7] showed that the critical impact energy depends on projectile nose radius. Wingrove[8] showed that blunt projectiles penetrated the target with least resistance followed by hemispherical and ogive penetrators in that order as long as the target thickness to projectile diameter ratio was less than one. Wilkins[9] found that sharp impactors have lower ballistics limits than blunt impactors when tested on thick metal plates while the opposite was found for thinner targets. Othe[10], *et al*. found that critical perforation energy for blunt and hemispherical impactors is higher than that for conical impactors. Experimental results by Zukas[11] indicated that more blunt the nose shape is, the higher is the ballistic limit velocity. Hence, more work is necessary to understand the problem well.

In the present work, the failure mechanisms such as radial crack propagation, petal formation, and delamination process in a normal impact using drop mass setup is discussed. Based on the experimental observations, analysis of laminated composite plates at normal impact is carried out. The analysis considers the petal formation and radial crack propagation process. The bending of the petals during the penetration process is modelled using plastic hinges permitting the evaluation of energy absorbed during this stage. It is observed that no plate dishing occurred in composite laminates as in the case of metallic plates.

2. EXPERIMENTAL PROCEDURE

The experiments on the penetration of chopped glass strand mat–polyester composite plates were conducted using a free-fall drop-weight fixture, and drop height in these experiments was 4 m, thus giving impact velocity in the range 2 m/s to 8 m/s. The fully-clamped tested square plates have side length of 310 mm and thickness 3.1 mm. The plates were made of six layers of chopped glass strand mat-350 with general purpose polyester resin available in the market. Photodiode-based digital time counter was used to find the impact velocity.

The impactors were made of mild steel, and their shapes were conical, cylindrical, and their combinations with varying nose diameters. Maximum dia of the impactors was 40 mm and length of conical portion was 50 mm. Nose shapes of conical impactors were 10 mm and 5 mm hemispherical and 10 mm blunt. Length of cylindrical impactor was 100 mm and dia was 40 mm. Schematic diagram of these impactors and the corresponding failure patterns are shown in Fig. 1. The impactors were attached to the circular discs of mass 20 kg, which were dropped through a pulley arrangement from different heights. Experiments were carried out for each impactor at different velocities. An anti-rebound mechanism was used to avoid multiple strikes on the specimen. Impactor pull out test was conducted to find the frictional energy.

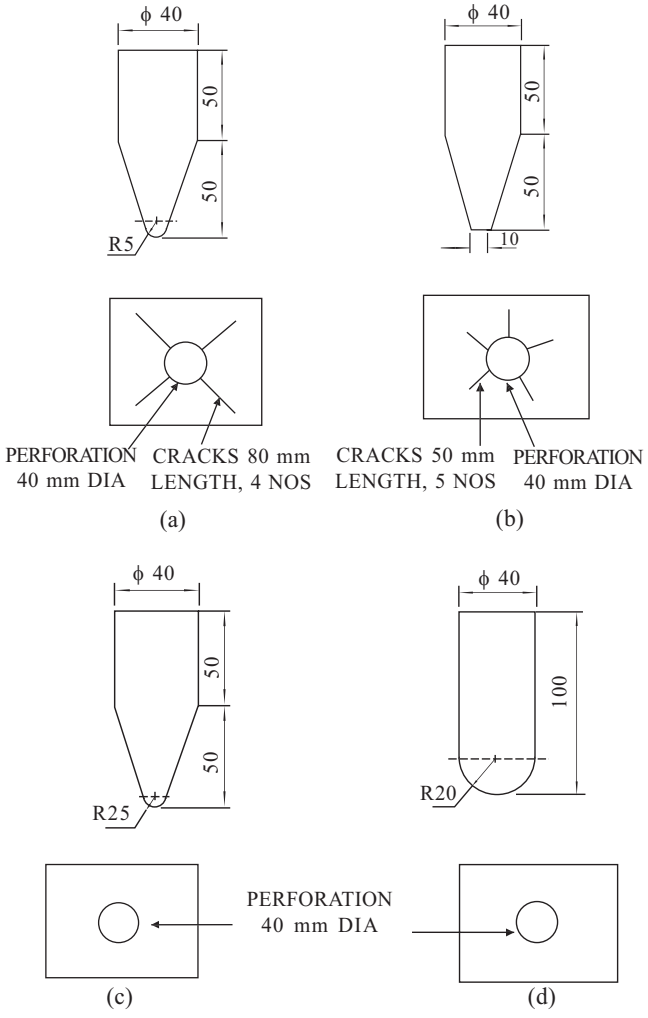

Figure 1. General failure pattern under different impactors: (a) conical impactor with 10 mm hemispherical nose; (b) conical impactor with 10 mm blunt nose; (c) conical impactor with 5 mm hemispherical nose; and (d) cylindrical impactor with 40 mm hemispherical nose.

To find the percentage of elongation and strength of the laminate, sample specimens were prepared according to ASTM D 3039 and subjected to uniaxial tension. Samples were also prepared according to ASTM D 2344 to find the shear strength and subjected to 3 point bending test. Sample specimens of 5 each were tested and their average value is taken for analysis.

3. ANALYSIS

Various failure modes observed from the experiments are plate bending, delamination of layers, and extension of cracks in the radial direction. It is seen that there is bending of petals at a radius equal to the radius of the impactor after the plate is perforated. Analytical expressions are formulated to find out the energy absorbed in these failure modes. After partial penetration, the moving nose of the impactor tends to enlarge the hole size, and thus, the cracks subsequently propagate outwards under the pressure of the impactor. The hoop stress is thus responsible for further radial extension of cracks.

From the tested plates it is observed that delamination causes the initiation of failure process. When delamination occurs, the debonded area generally is of circular shape with the maximum crack length as radius. Thus, the delamination energy involved in the process is given by the expression

$$U_{del} = \int \tau \varepsilon_d \, dV \tag{1}$$

Volume of the delaminated material is $\pi a^2 h_0$ and the expression for ε_d is

$$\varepsilon_d = \delta_d / a \tag{2}$$

From Eqns (1) and (2), total delamination energy is obtained from the expression

$$U_{del} = \tau \pi a h_o \delta_d \tag{3}$$

where δ_d is the vertical deformation which is obtained from 3 point bending test and a is the maximum crack length.

The hoop strain energy required for formation of one crack is

$$U_{hoop} = \sigma_y \varepsilon_h \pi a^2 h_0 \tag{4}$$

where, σ_y is the maximum hoop stress and ε_h is the maximum strain corresponding to uniaxial tension as the failure mode of hoop strain is in tension.

During the outward crack propagation, there will be parallel outward motion of cracks in the petals until the cracks are arrested and arrive subsequently at the root of the petal as shown in Fig. 2.

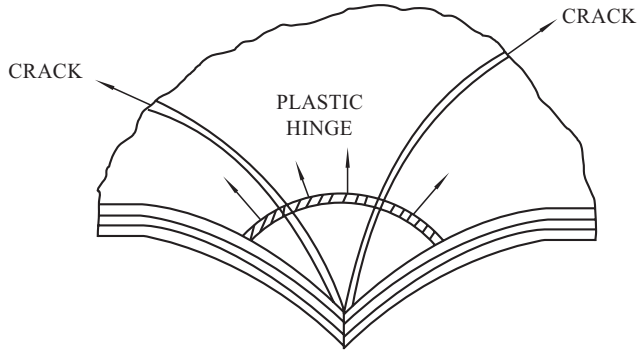

Figure 2. Propagation of cracks and plastic hinge.

To calculate the petal rotational energy, a petal is assumed as a triangular cantilever beam with constant thickness h_0 and length a. The beam behaviour is similar to that of an isotropic material with the plastic hinges at the root. Hence the petal rotational energy is calculated by calculating the maximum bending moment involved in bending of petals. It is expressed as

$$M_p = \sigma_y Z_p \tag{5}$$

For a triangular beam with constant thickness

$$Z_p = \frac{B h_0^{\,2}}{4} \quad \text{and} \tag{6}$$

$$B = \frac{2\pi a}{n} \tag{7}$$

Substitution of Eqns (6) and (7) in Eqn (5) gives the total plastic bending moment of one petal given by

$$M_p = \frac{\sigma_y B h_0^{\,2}}{4} \tag{8}$$

After the arrest of crack at the root of the petals, the moving mass and petals still possess kinetic energy and therefore additional rotation of petals takes place about its root by an angle θ_2–θ_1, which is sufficient for the free passage of the impactor.

Figure 3 shows this mechanism. The angle $\theta_2 - \theta_1$ can be calculated from the geometry considering the extension of a petal. In most of the cases, it will be close to 90°. Therefore the plastic rotational energy of one petal is given by

$$U_p = M_p \theta = \frac{\sigma_y B h_0^{\,2} \pi}{8} \tag{9}$$

To obtain the total petal rotational energy, the above expression has to be multiplied with the number of petals.

Frictional energy has been neglected in the previous investigations assuming that it is negligible[15,16]. But, it is found that this energy cannot be neglected in composite structures as it has significant contribution in the energy dissipation.

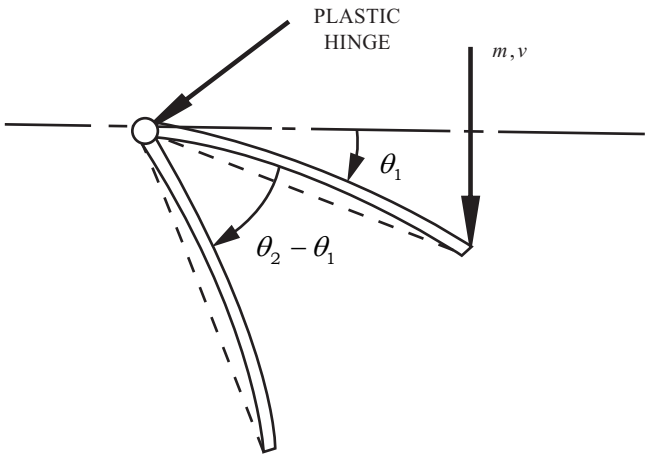

Figure 3. Arrival of plastic hinge at the root of the petal and subsequent rotation.

Total frictional energy is given by the expression,

$$U_f = pl \tag{10}$$

where p is assumed to be the impactor pullout force obtained from static experiments and l is the length of the impactor. Also the dynamic frictional coefficient is less than the static coefficient and is assumed as 0.8 times the static frictional coefficient, hence Eqn (10) becomes

$$U_f = 0.8\,pl \tag{11}$$

Equations (3), (4), (9), and (11) provide the total strain energy absorbed by the plate by various failure modes.

4. RESULTS AND DISCUSSION

Five sets of composite plates were tested under each impactor. The applied energy was varied by varying the drop height. All the specimens tested have a tensile breaking strength of 133.33 N/mm^2. The fibre volume fraction was 32 per cent. Maximum elongation observed in tension test is 0.57 mm. Short beam bending tests were carried out to find out the shear strength and the value is 55.46 N/mm^2.The stress strain curve of the laminate when subjected to uniaxial tension test is shown in Fig. 4(a). Figure 4(b) shows an impactor used along with drop mass and Fig. 4(c) shows the tested specimen along with the impactor after removing from the rig. Quasi-static load is applied to remove the impactor which is considered as the frictional load for analysis.

Various energy values obtained from plates tested with conical impactor of 10 mm dia hemispherical nose are given in Table 1. It is clear from this table that hoop strain energy is the predominant one since the cracks have extended beyond perforation.

From the tested specimens it is seen that there are 4 cracks in all the tested plates under conical impactor of 10 mm dia hemispherical nose. In plate Nos. 1 and 2, the failure mechanisms are identical even though the energy applied was different and the crack lengths are 80 mm. The general pattern is shown in Fig. 1(a). Hence, it is clear that

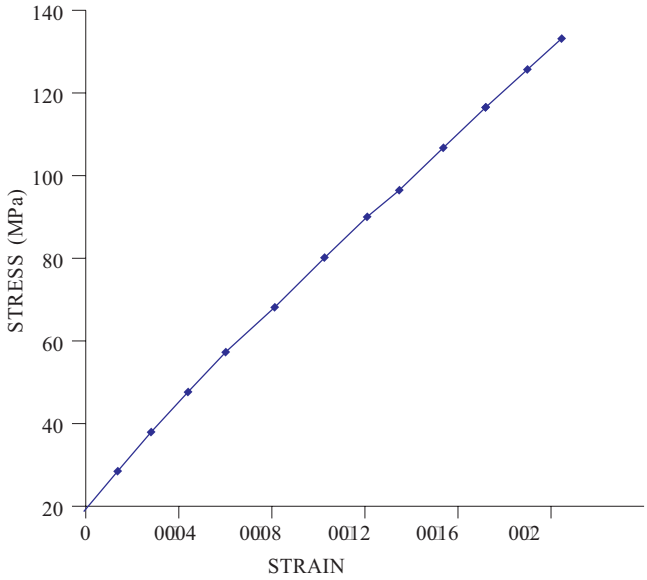

Figure 4(a). Stress-strain curve for the laminate subjected to uniaxial tension.

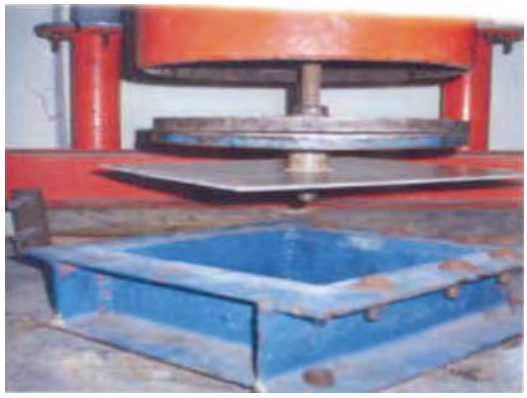

Figure 4(b). Test rig with tested specimen.

Figure 4(c). Perforated plate with impactor.

Table 1. Various energies obtained from plates tested with conical impactor of 10 mm hemispherical nose

Impactor type	Plate no.	Hoop strain energy (N-m)	Petal rotational energy (N-m)	Delamination energy (N-m)	Frictional energy (N-m)	Total energy absorbed (N-m)	Applied energy (N-m)
Conical with 10 mm dia hemispherical nose	1	194.19	55.80	45.50	48.00	343.5	710.00
	2	194.19	55.80	45.50	48.00	343.5	507.60
	3	94.810	55.80	30.90	28.80	210.00	304.60
	4	55.70	55.80	22.34	28.80	163.50	203.30
	5	18.40	23.70	15.70	28.80	86.90	101.50

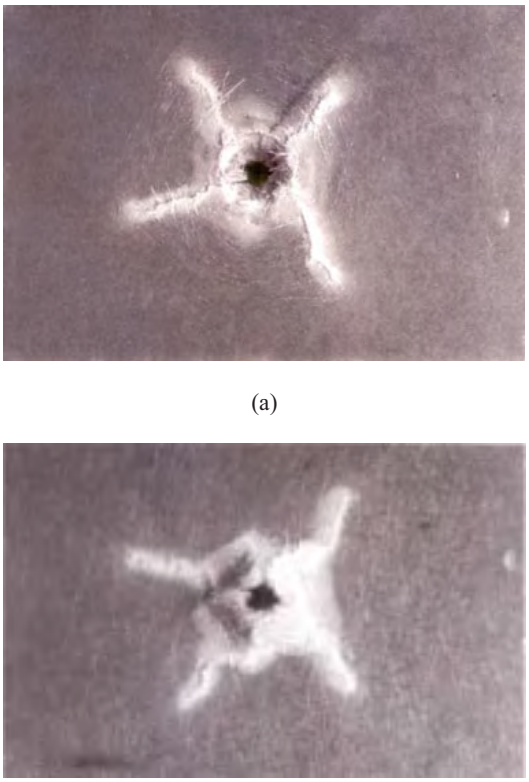

(a)

(b)

Figure 5. Surface of plate impacted with 10 mm hemispherical-nosed impactor: (a) Top surface and (b) bottom surface.

increase in impact energy beyond a certain limit does not increase the damage zone. In all the tests, the perforation hole size is exactly the size of the impactor. So, complete petal rotation takes place only at a distance equal to the maximum radius of the impactor. This can be seen from Figs 5(a) and 5(b) which show the top and bottom surfaces of the plate. Also, it is observed that the cracks at bottom layers are longer than that of top layers. When the applied energy was further reduced, i.e., the drop height was reduced to 1.5 m and 1.0 m, there was no crack extension beyond the perforation. In plate no. 5, in which the weight was dropped from the height of 1 m and the impact energy was only 101.5 N-m, the number of petals is reduced to 3 and perforation dia also reduces, i.e., the impactor did not perforate fully. It is also observed that if the impact energy is still less, there will be only delamination over the central zone.

Plate nos. 6 to 10 were tested with conical impactor of 10 mm dia blunt-ended nose. Values of various energy terms obtained from the plates tested with this impactor are given in Table 2. From this table it is clear that petal rotational energy is more than hoop strain energy. The delamination energy is less when compared to corresponding energy in Table 1.

Plate no. 6 was tested at a height of 3.5 m with energy of 710 N-m. The failure pattern was compared with plate No. 1 which was tested with an impactor having 10 mm dia hemispherical nose. The maximum crack length in plate no. 6 was 50 mm and in plate no. 1, it was 80 mm. This shows that crack length decreases with increase in contact area. Number of cracks in plate nos. 6, 7, 8, and 9 was 5. Hence, as the contact area of the impactor increases, there is decrease in crack length and number of cracks increases from 4 to 5 (Fig. 1(b)). Figures 5(c)-5(d) show the top and bottom surfaces of the plates impacted with blunt nose. As observed in previous case, the perforation size is the size of the impactor. As the drop height is reduced, there is no crack extension beyond the perforation, which is seen in plate nos. 7, 8, 9, and 10. At higher energies, the delamination zone is found to be higher for

Table 2. Various energies obtained from plates tested with conical impactor of 10 mm blunt-ended nose

Impactor type	Plate no.	Hoop strain energy (N-m)	Petal rotational energy (N-m)	Delamination energy (N-m)	Frictional energy (N-m)	Total energy absorbed (N-m)	Applied energy (N-m)
Conical with 10 mm dia blunt-ended nose	6	93.30	72.50	30.30	48.00	244.10	710.00
	7	48.34	72.50	23.40	48.00	192.2	507.60
	8	48.34	72.50	18.12	28.80	167.64	304.60
	9	30.45	58.50	15.23	28.80	132.93	203.30
	10	8.00	32.40	10.97	28.80	80.20	101.50

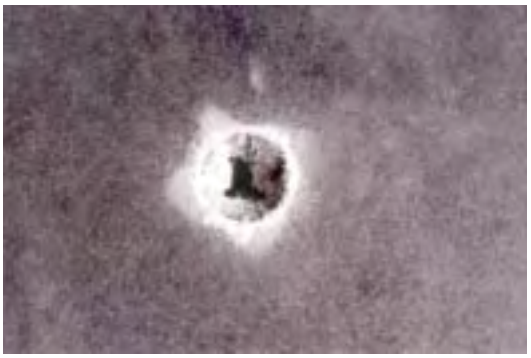

(c)

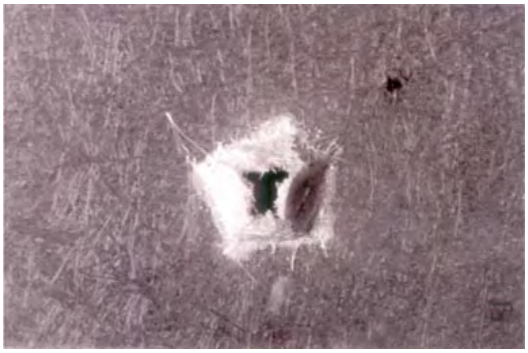

(d)

Figure 5. Plate impacted with 10 mm blunt-nosed impactor: (c) top surface and (b) bottom surface.

hemispherical-ended impactors than that of blunt-ended impactors. At lower energies, blunt-ended impactors cause more delamination than the hemispherical-ended impactors.

Plate nos. 11 to 15 were tested with conical impactor of 5 mm hemispherical nose. Values of various energy terms obtained from the tested plates are given in Table 3. From this table, it can be seen that hoop strain energy and delamination energy reduced significantly and petal rotational energy increased when compare with Tables 1 and 2. Frictional energy is almost the same in all the four impactors.

Plate no. 11 was tested with an energy of 710 N-m. Unlike in plates 1 and 6, there is no crack extension beyond the perforation at all energy levels. The general crack pattern is shown in Fig. 1(c). Perforation followed the same size and geometry of the impactor as seen in other plates. Number of petals in the plate due to 10 mm hemispherical nose is 4 and for 5 mm nose dia, it is 7. As seen earlier, the crack length at the bottommost layer is more than that appeared at the top surface since the bottom layers delaminated more. Figures 5(e)-5(f) show the top and bottom

Table 3. Various energies obtained from plates tested with conical impactor of 5 mm hemispherical-ended nose

Impactor type	Plate no.	Hoop strain energy (N-m)	Petal rotational energy (N-m)	Delamination energy (N-m)	Frictional energy (N-m)	Total energy absorbed (N-m)	Applied energy (N-m)
conical with 5 mm dia hemispherical nose	11	32.65	79.00	12.65	48.00	172.30	710.00
	12	32.65	79.00	12.65	48.00	172.30	507.60
	13	32.65	79.00	12.65	48.00	172.30	304.60
	14	25.29	71.00	11.13	28.80	136.20	203.30
	15	13.37	50.00	8.07	15.84	87.28	101.50

surfaces of the tested plates. Unlike in plate Nos 1-10, there is no ring crack mechanisms found in the perforated plates tested with conical impactor of 5 mm nose dia since there is no crack extension beyond the perforation diameter. When the impact energy was reduced, the diameter of penetration also decreased since the impactor did not pass through the laminate fully and the number of petals remained 7. The same was observed in all the plates tested with impactor of 5 mm nose dia.

(e)

(f)

Figure 5. Plate impacted with 5 mm hemispherical-nosed impactor: (e) top surface and (f) bottom surface.

Various energy values obtained from plates tested under cylindrical impactor of 40 mm dia are given in Table 4. Petal rotational energy is more when compare with the similar previous cases. Delamination energy is more than that in the case of conical impactor of 5 mm hemispherical nose. In all the tested plates, number of petals is 4. The size of the petals is not uniform unlike in other plates. It is observed that the perforation has followed the same geometry of the impactor and there are no extended cracks beyond the perforation even at higher energies. The general crack pattern is shown in Fig. 1(d). The failure pattern is the same in all the plates tested at different heights. There are always two larger petals and two smaller petals. It is seen that the delamination area at the bottom of the plates tested by 40 mm dia impactor is much higher than that tested by other impactors. Hence, the width at the root and crack length are more for these petals. Figures 5(g)-5(h) show the top and bottom surfaces of the tested plates.

Figures 5(i) and 5(j) are the top and bottom views of the plate impacted at lower energy with 10 mm dia hemispherical nose. The failure pattern shown in these figures are observed in all the tests done under different impactors at lower energies. From these, it can be seen that at lower energy, delamination is more and number of petals is less. Also there are many number of internal concentric ring cracks in the damaged zone.

From Figures 5(a) - 5(j), it is clear that the top and bottom surfaces of the plates have different failure mechanisms. For all the tests done at higher energy levels, at the top surface there is perforation and delamination and at the bottom surface, in addition, there is petal formation also. At lower energy levels,

Table 4. Various energies obtained from plates tested with cylindrical impactor of 40 mm dia hemispherical nose

Impactor type	Plate no.	Hoop strain energy (N-m)	Petal rotational energy (N-m)	Delamination energy (N-m)	Frictional energy (N-m)	Total energy absorbed (N-m)	Applied energy (N-m)
Cylindrical with 40 mm dia hemispherical nose	16	60.20	110.70	30.36	48.00	249.26	710.00
	17	57.47	96.40	25.77	48.00	227.64	507.60
	18	46.43	90.14	25.30	48.00	209.87	304.60
	19	43.62	80.48	22.77	28.8	175.67	203.30
	20	23.47	60.48	10.24	0.0	94.19	101.50

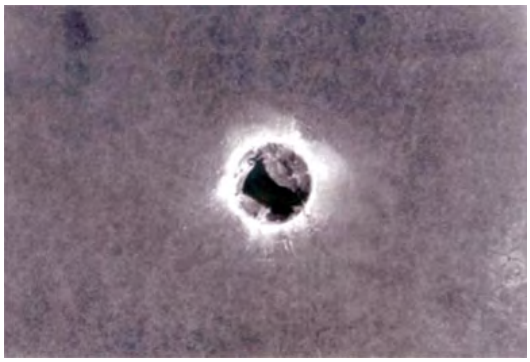

(g)

(h)

Figure 5. Plate impacted cylindrical impactor with 40 mm dia hemispherical nose: (g) top surface and (h) bottom surface.

except in the case of plates tested under 5 mm hemispherical-nosed impactor, there is only matrix crack at the top surface and in the bottom surface, one can see that in addition to matrix crack, there is fibre breakage (Figs 5(i) and 5(j)). The ring cracks are only partial since they are not rotated fully and complete fibre breakage has not occurred.

Comparison of total energy absorbed by the plate due to different impactors is shown in Fig. 6. The variation indicates that when the nose is sharp, energy absorbed is less and if the nose is wide enough to have increased contact area, energy absorption is more.

Frictional energy is calculated using Eqn (11) and is given in Tables 1-4 for different impactors. These values show that this energy cannot be neglected in the impact perforation phenomena.

(i)

(j)

Figure 5. Plate impacted at lower energy with 10 mm dia hemispherical nose: (i) top surface and (j) bottom surface.

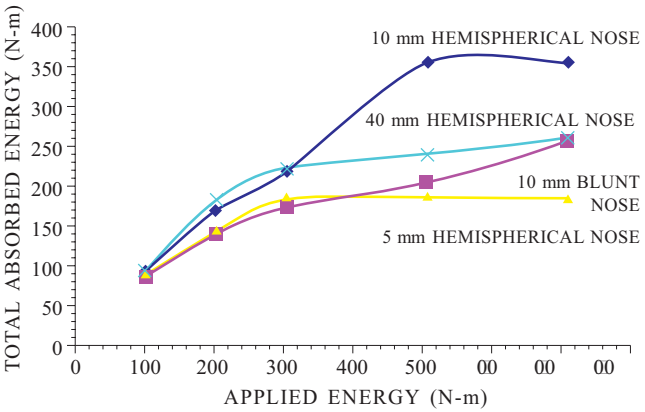

Figure 6. Comparison of total energy absorbed from different impactors.

5. CONCLUSIONS

A simple method to find the energy absorption in the perforation process of laminated panels by conical impactors has been established. This approach is based on the work done in crack formation,

delamination and petal bending. The influence of contact area in energy absorption is also investigated. From experiments, it is found that the damage area can not be increased beyond a certain value of impact energy. The perforation hole size is equal to the maximum diameter of the impactor irrespective of increased crack length and complete rotation of petals takes place at a distance of radius of the impactor from the central point of the impact zone. The length of cracks in the bottom layers is more than that in the top layers.

It is also observed that the crack length and number of petals vary with variation in contact area. Number of cracks is more when impactor nose is almost sharp. When impactor nose is either sharp (5 mm nose dia) or contact area is much high (40 mm dia), there is no extended cracks beyond perforation even at higher energies. At lower energies, blunt-ended impactors cause more delamination than that by a hemispherical impactor, and at higher energies, it is in the reverse order. From the experiments and analysis, it is clearly observed that friction between the impactor and plate has to be considered for the analysis as the frictional energy is not negligible. It is found that there exists many numbers of visible concentric circular partial plastic hinge mechanisms at the top surface of plates.

REFERENCES

1. Serge, Abrate. Impact on composite structures. Cambridge University Press, Cambridge, 1998.
2. Choi, H.Y. & Chang, R.K. A model for predicting damage in fraphite/epoxy laminated composites resulting from low velocity point impact. *J. Composite Mater.,* 1992, **26,** 134-69.
3. Davis, G.A.O. & Zhang, X. Impact damage prediction in carbon composite structures. *J. Impact Engg.*, 1995, **16**, 149-70.
4. Landkof, B. & Goldsmith, W. Pedaling of thin metallic plates during penetration by cylindro-conical projectiles. *J. Solid Struct.*, 1985, **21**(3), 245-66
5. Gupta, N.K. & Madhu, V. Normal and oblique impact of a kinetic energy projectile on mild steel plates. *Int. J. Impact Engg.,* 1992, **12**, 333-43.
6. Corran, R.S.J.; Shadbolt, P.J. & Ruiz, C. Impact loading of plates: An experimental investigation. *Int. J. Impact Engg.*, 1983, **1**, 3-22.
7. Johnson, W. Impact strength of materials. Edward Arnold Publishers, London, 1972.
8. Wingrove, A.L. The influence of projectile feometry in adiabatic shear and target failure. *Metall. Mater. Trans.*, 1973, **A**(4), 1829-833.
9. Wilkins, M.L. Mechanics of penetration and perforation. *Int. J. Engg. Sci.*, 1978, **16**, 793-807.
10. Othe, S.; Yoshizava, H.; Chiba, N. & Shida, S. Impact strength of steel plates struck by projectiles. *Bulletin JSME,* 1982, **25**(205), 1226-231.
11. Zukas, J.A., *et al.* Impact dynamics. Krieger Publishing Co, New York, 1972.
12. Goldsmoth, W. & Calder, C.A. Plastic deformation and perforation of thin plates resulting from projectile impact. *Int. J. Solids Struct.,* 1971, **7**, 863-68.
13. Davis, G.A.O.; Hitchings, D. & Wang, J. Prediction of threshold impact energy for onset of delamination in quasi-isotropic carbon/epoxy composite laminates under low velocity impact. *Comp. Sci. Technol.*, 2000, **60**, 1-7.
14. Giovanni, B. & Roberto, V. Low velocity impact tests of laminate glass fibre epoxy matrix composite material plates. *Int. J. Impact Engg.*, 2002, **27**(2), 213-29.
15. Serge, Abrate. Impact on laminated composite materials. *Amer. Soc. Mech. Engrs. (ASME)*, 1991, **4**(44), 155-90.
16. Christoforou, Andreas, P. Impact dynamics and damages in composite structures. *Composite Structures*, 2001, **52**, 181-88.
17. Kim, Jang-Kyo & Sham, Man-Lung. Impact and delamination failure of woven fabric composites. *Comp. Sci. Technol.*, 2000, **60**, 745-61.

Contributor

Dr R. Velmurugan obtained his ME (Aerospace Engg) from Indian Institute of Science, Bangalore, in 1990 and PhD (Large Deformations) from Indian Institute of Technology (IIT) Delhi, New Delhi. He worked as Asst Prof at the Mepko Schlenk Engineering College, Sivakasi, and IIT Madras, Chennai. Presently, he is Assoc Prof at IIT Madras, Chennai. He has about 40 research papers presented/ published in various national and international conferences and journals. He has completed two sponsored research projects of Armmament Research & Development Board (AR&DB), New Delhi, and the Combat Vehicle Research & Development Estt, Avadi, and has an ongoing research project from Defence Research and Development Laboratory, Hyderabad.